Coastal Engineering Journal

ISSN: (Print) (Online) Journal homepage: https://www.tandfonline.com/loi/tcej20

Application of the WRF model to the coastal area at Ise Bay, Japan: evaluation of model output sensitivity to input data

Yoshitaka Matsuzaki, Takashi Fujiki, Koji Kawaguchi, Tetsunori Inoue & Takumu Iwamoto

To cite this article: Yoshitaka Matsuzaki, Takashi Fujiki, Koji Kawaguchi, Tetsunori Inoue & Takumu Iwamoto (2021) Application of the WRF model to the coastal area at Ise Bay, Japan: evaluation of model output sensitivity to input data, Coastal Engineering Journal, 63:1, 17-31, DOI: 10.1080/21664250.2020.1830485

To link to this article: https://doi.org/10.1080/21664250.2020.1830485

COASTAL ENGINEERING JOURNAL
2021, VOL. 63, NO. 1, 17–31
https://doi.org/10.1080/21664250.2020.1830485

ORIGINAL RESEARCH PAPER

OPEN ACCESS Check for updates

Application of the WRF model to the coastal area at Ise Bay, Japan: evaluation of model output sensitivity to input data

Yoshitaka Matsuzaki[a], Takashi Fujiki[b], Koji Kawaguchi[b], Tetsunori Inoue[a] and Takumu Iwamoto[b]

[a]Marine Environment Control System Department, Port and Airport Research Institute, Yokosuka, Japan; [b]Ocean Hydrodynamics Department, Port and Airport Research Institute, Yokosuka, Japan

ABSTRACT

WRF simulations were conducted for Ise Bay, Japan for January and July 2016 to evaluate sensitivity of model input and output above sea surface to the replacement of three default input datasets with region-specific input datasets. For atmospheric input data, a final analysis created by the National Centers for Environmental Prediction (NCEP-FNL) was replaced with a mesoscale analysis created by the Japan Meteorological Agency (JMA). Topography and land use dataset released by the US Geological Survey were replaced with dataset released by the GeoSpatial Information authority of Japan. For sea surface temperature (SST) data, NCEP-FNL was replaced with an analysis created by JMA. Of the three region-specific datasets, replacement of atmospheric data results in the largest improvements in the accuracy of simulated wind speeds in January and July and of temperature in July 2016. Improvements in model output accuracy over sea surface can be seen near the coastline by replacing topography and land use data. Replacement of SST data results in the largest improvements in simulated temperature accuracy in January 2016. Replacing all three default input datasets results in the largest improvement, and expands on results from previous studies that focused on the effects of replacing only one input data.

ARTICLE HISTORY
Received 22 May 2020
Accepted 27 September 2020

KEYWORDS
WRF; wind speed; temperature; above sea surface; Ise Bay

1. Introduction

The coastal environment is affected by atmospheric forcing. For example, strong wind blowing toward the mouth of a bay causes upwelling of bottom water at the head of a closed bay (e.g. Higa et al. 2015; Lai et al. 2016). Air temperature is closely related to water temperature, which affects the metabolic activities of coastal organisms such as sea grass, zooplankton, and phytoplankton. Thus, accuracy of the atmospheric forcing data is very important for accurate numerical simulations of coastal environments.

Final analysis of a weather model created by the National Centers for Environmental Prediction (NCEP-FNL) (National Centers for Environmental Prediction/National Weather Service/NOAA/U.S. Department of Commerce 2015) can be considered as a default atmospheric forcing data for numerical simulations of coastal environments. However, around Japan, longitudinal and latitudinal resolutions of NCEP-FNL are about 23 and 28 km, while horizontal grids of simulations of coastal environments are on the order of several hundred meters; therefore, resolution of NCEP-FNL dataset is insufficient for the simulation of local current velocity and water temperature. Downscaling NCEP-FNL dataset using a weather model, such as the mesoscale numerical weather simulation system Weather Research and Forecast (WRF) model (Skamarock et al. 2008) can produce atmospheric forcing data with high spatial and temporal resolutions that can be used in simulations of coastal environments.

Previous studies reported that accuracy of WRF output varies with input data, which can be roughly classified into three types: (a) atmospheric data (e.g. Akimoto and Kusaka 2010; Carvalho, Rocha, and Gómez-Gesteira 2012; Misaki et al. 2019), (b) topography and land use (e.g. Cheng et al. 2013; Jee and Kim 2016; Jiménez-Esteve et al. 2018; Mallard, Spero, and Taylor 2018; Kikuchi, Fukushima, and Ishihara 2020), and (c) sea surface temperature (SST) as a lower boundary condition (e.g. LaCasse et al. 2008; Song et al. 2009; Shimada et al. 2015; Kikuchi, Fukushima, and Ishihara 2020). Studies focused on coastal areas are reviewed in the following section. Carvalho, Rocha, and Gómez-Gesteira (2012) conducted WRF simulations using three atmospheric reanalysis datasets to simulate surface oceanic wind offshore of the Iberian Peninsula. They concluded that local winds were simulated accurately and realistically when atmospheric input data that are representative of local conditions were used. Misaki et al. (2019) conducted WRF simulations using three atmospheric datasets to evaluate accuracy of WRF simulated wind speeds above the sea surface in Niigata and Ibaraki, Japan. Kikuchi,

CONTACT Yoshitaka Matsuzaki matsuzaki-y@p.mpat.go.jp

Fukushima, and Ishihara (2020) conducted WRF simulations for the area around the offshore observation station (meteorological mast) at Choshi, Japan to evaluate the effect of replacing the land use dataset from the US Geological Survey (USGS) by the high resolution dataset provided by the National Land Information Division. Use of the land use data reduced overestimation of the north wind, which blows from land to sea. Kikuchi, Fukushima, and Ishihara (2020) also conducted WRF simulations using bias corrected SST dataset, and reported reduced overestimation of the southwest wind. Song et al. (2009) conducted WRF simulations using different SST datasets and indicated the importance of SST resolution for accurate simulation of surface wind speed. Shimada et al. (2015) reported that accurate simulation of winds above the sea surface required SST data that are close to field values. Their focus was on the improvement of simulated results by replacing default atmospheric, topography and land use, and SST input data; they did not identify the input data type, which, when replaced, would result in large improvements in simulation results. Furthermore, while previous studies have each focused on one of the three input data types, no study has yet examined the combined effect of replacing the default data of all three data types.

In this study, comparisons between WRF simulation results and observations above the sea surface in Ise Bay, Japan were conducted for evaluating sensitivity of model output to the three types of region-specific input data. First, bias, correlation, and root mean square error (RMSE) between observations and model input were calculated for wind speed, air temperature, and SST. Second, these three indices between observations and model output were calculated for wind speed and air temperature. Moreover, the combined effects of replacing default datasets of three input data types with region-specific datasets in improving model output accuracy were verified. Results of this study provide useful guidance for coastal WRF simulations.

2. Materials and methods

Simulations were conducted using WRF version 3.7.1 to evaluate sensitivity of model output above the sea surface in Ise Bay, Japan to input data (Figure 1). Ise Bay has a surface area of 1,730 km^2 and extends across approximately 70 km in both the longitudinal and latitudinal directions.

In this study, three types of default input dataset were replaced with region-specific dataset; the three types are: (a) atmospheric data, (b) topography and land use, and (c) SST; their specifications and characteristics are summarized in the following sections.

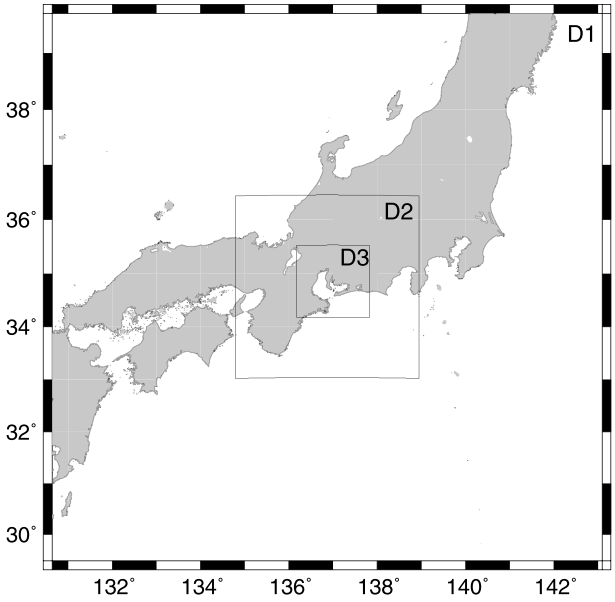

Figure 1. WRF domains. Domain 3 includes Ise Bay.

2.1. Atmospheric data

2.1.1. Default dataset: National Centers for Environmental Prediction Final analysis (NCEP-FNL)

The NCEP-FNL operational global analysis and forecast dataset are on 0.25°×0.25° grids, prepared every 6 hours, and are available at 26 vertical levels (National Centers for Environmental Prediction/National Weather Service/NOAA/U.S. Department of Commerce 2015); over the Ise Bay region, the grid is about 23 and 28 km in the longitudinal and latitudinal directions. This product is from the Global Data Assimilation System, which continuously collects observational data from the Global Telecommunications System and other sources for many analyses.

2.1.2. Region-specific dataset: Japan meteorological agency meso-scale analysis (JMA-MA)

The JMA-MA is on 0.05°×0.0625° grids, and has 48 vertical levels. It is prepared every 3 hours, and distributed at 16 vertical levels. In the Ise Bay region, grid spacing is approximately 5 km. Accuracy was improved through the four-dimensional variational data assimilation of observation data, e.g. pressure, temperature, wind, humidity, precipitation, and radiation (Japan Meteorological Agency 2016).

2.2. Topography and land use

2.2.1. Default dataset: U.S. geological survey (USGS)

The USGS GTOPO30 is a global digital elevation model with a horizontal grid spacing of 30 arc seconds. Land use data were obtained from the USGS Global Land Cover Characteristics database (Loveland et al. 2000),

Table 1. Correspondence list of land use classifications. This list is based on Sashiyama and Yamamoto (2014).

USGS	GSI	GSI (Urban areas)
Urban and Built-up Land	Building	Road
	Road	Railway
	The other uses (e.g. Athletic field)	
Irrigated Cropland and Pasture	Rice field	Rice field
Cropland/Grassland Mosaic	Wasteland	Wasteland
Grassland	Other farmlands	Other farmlands
	Golf course	Golf course
		Open space
		Park and greenery area
Mixed forest	Forest	Forest
Water bodies	River and lake	River and lake
	Seashore	Seashore
	Sea	Sea
Low Intensity Residential		Low residential
		Low intensity residential (crowded)
High Intensity Residential		High intensity residential
Industrial of commercial		Factory
		Public facilities

which was developed through an unsupervised classification of 1 km Advanced Very High-Resolution Radiometer (AVHRR) satellite data (Sertel, Robock, and Ormeci 2010).

2.2.2. Region-specific dataset: geospatial information authority of Japan (GSI)

Topography and land use data of Japan are provided by the GeoSpatial Information authority of Japan (GSI). Topography data are created by interpolating altitude values obtained from contours on GSI's 1/25,000 topographic maps; horizontal grid spacing is 10 m; accuracy of altitude, as measured by standard deviation, is within 5.0 m. Land use data are created from an electronic base map of Japan and satellite observations (e.g. SPOT, RapidEye, Advanced Land Observing Satellite – ALOS); horizontal grid spacing is 100 m. The WRF model uses land use categories in USGS, which are different from those in the GSI dataset. Therefore, GSI land use categories were reclassified as USGS categories following the correspondence list of Sashiyama and Yamamoto (2014) (Table 1). Figure 2 shows land use category in each grid cell around Ise Bay in model domain 3, which has a horizontal grid size of 800 m. In coastal areas, USGS dataset indicates dominance of cropland and grassland while GSI dataset indicates dominance of low and high residential areas. The GSI dataset also correctly capture the boundary between land and sea, including small islands and the offshore airport in Ise Bay. Therefore, we consider that GSI dataset are suitable as input for WRF simulations in coastal areas.

2.3. Sea surface temperature (SST)

2.3.1. Default dataset: NCEP-FNL

Skin temperature from NCEP-FNL can be used as SST input data for WRF. Since January 14, 2015, NCEP-FNL has included a high-resolution version of NCEP real-time global SST (Thiébaux et al. 2003) with a horizontal resolution of 1/12°, which corresponds to about 8.3 km in the Ise Bay region. These dataset have the additional advantage of using SSTs obtained from AVHRR using a physical stochastic retrieval methodology that reduces regional biases due to local atmospheric conditions (Gemmill, Katz, and Li 2007); in-situ data from moored and drifting buoys are also used to remove residual biases in the satellite SST field (Maturi et al. 2017).

2.3.2. Region-specific dataset: JMA ocean model for Region North Western Pacific (JMA-RNWPA)

Dataset from JMA's multivariate ocean variational estimation system/meteorological research institute community ocean model (Usui et al. 2006) for Region North Western Pacific (JMA-RNWPA) are on 0.1°×0.1° grids, prepared every day, and are available at 52 vertical

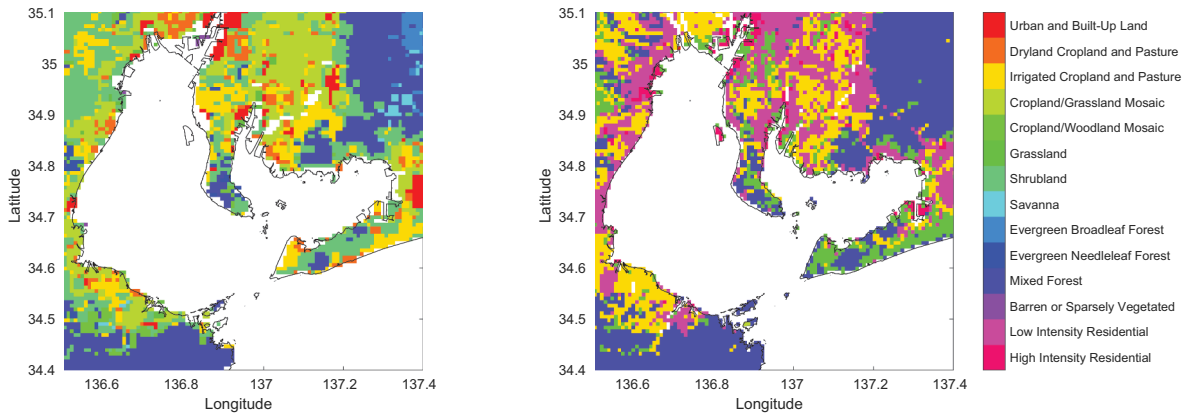

Figure 2. Land use categories around Ise Bay in domain 3 (horizontal grid size 800 m) from USGS (left) and GSI (right). White color indicates water bodies. Black line indicates coastline. Only area around Ise Bay in domain 3 is shown.

levels. A multivariate three-dimensional variational analysis scheme with vertical coupled temperature-salinity empirical orthogonal function modes is used, and three variables are assimilated: water temperature and salinity measured near sea surface using ships, buoys, ARGO floats, or other means, and sea surface height obtained from satellite data. In the Ise Bay region, grid spacing is approximately 10 km. Water temperatures closest to sea surface (at a depth of 1 m) were used as SST input data for WRF simulations.

2.4. Experimental set-up

Sensitivity analyses were conducted for five cases. Table 2 shows the input data used in each case. In the standard experiment (case 1), default input dataset were used; atmospheric initial and boundary conditions, assimilation value for four dimensional data assimilation (FDDA), SST (i.e. lower boundary conditions), and land surface boundary conditions were taken from NCEP-FNL; topography and land use data were taken from USGS. In the four sensitivity experiments (cases 2–5), default input datasets were replaced by region-specific datasets. In case 2, NCEP-FNL was replaced with JMA-MA to evaluate model output sensitivity to the replacement of atmospheric input dataset. In case 3, USGS topography and land use dataset were replaced with GSI dataset. In case 4, the SST field in NCEP-FNL was replaced with JMA-RNWPA dataset. In case 5, all three input datasets in case 1 were replaced with those used in cases 2, 3, and 4. There are no land surface data in JMA-MA; therefore, for cases 2–5, NCEP-FNL dataset were used for land surface boundary conditions.

Table 3 shows the configuration for WRF simulations. Model domain covered central Japan, including Ise Bay as shown in Figure 1. There are three nested domains, and all domains interact with each other through a two-way nesting. Horizontal grid size in the innermost domain (D3) was set to 800 m to show differences between sea and land. In the preliminary simulations, WRF simulations were conducted without FDDA, but the scores were poor.

Table 2. Input data used in cases 1–5.

Case	Experimental conditions	Atmospheric input data	Topography and land use data	SST data
case 1	Standard experiment	NCEP-FNL	USGS	NCEP-FNL
case 2	Atmospheric input data are replaced	JMA-MA	USGS	NCEP-FNL
case 3	Topography and land use data are replaced	NCEP-FNL	GSI	NCEP-FNL
case 4	SST data are replaced	NCEP-FNL	USGS	JMA-RNWPA
case 5	All three input data are replaced	JMA-MA	GSI	JMA-RNWPA

Table 3. Model configuration for WRF simulations.

Model configuration			
Vertical resolution	40 levels (surface to 10 hPa)		
Nesting	Two way nesting		
Domain	Domain 1	Domain 2	Domain 3
Horizontal grid size	7200 m	2400 m	800 m
Dimensions	160 × 160	160 × 160	190 × 190
Time step	30 s	10 s	3.3 s
Physics options			
Surface layer	Revised MM5 surface layer		
Planetary boundary layer	YSU		
Short wave radiation	RRTMG		
Long wave radiation	RRTMG		
Microphysics	Thompson		
Cumulus parameterization	Kain–Fritsch	None	None
Land surface	Five-layer thermal diffusion		
Four dimensional data assimilation (FDDA)	enabled in all domains and grids.		

Thus, in this study, WRF simulations were conducted with FDDA, and the result of the preliminary simulations was used for the discussion of the effects of atmospheric data replacement on score improvement. We applied FDDA by grid nudging, and the nudging coefficient for the horizontal components of wind speed, temperature, and water vapor mixing ratio was set to 3.0×10^{-4} s^{-1}, which is the default value. Simulations were conducted over the entire months of January and July in 2016. There are two types of characteristic wind patterns in Ise Bay: from fall to spring, seasonal wind from the northwest, and in summer, land and sea breeze from the southeast in the day and from the northwest in the night (e.g. Sekine, Nakamura, and Wang 2002). Therefore, we chose January and July as representative months to capture the characteristics of the wind pattern in Ise Bay.

2.5. Accuracy validation methods

Accuracy of input data in the study area (around Ise Bay) is important for improving WRF simulated wind speed and temperature. Thus, first, input data (wind speed, air temperature, and SST) were compared with observation data from Ise Bay to validate model input accuracy.

Second, WRF output data (wind speed and air temperature) in the innermost domain (D3) were compared with observation data from Ise Bay mainly above sea surface. Comparisons were also conducted for data over land to allow the effects of replacing default topography and land use dataset to be discussed.

Figure 3 shows the locations of all observation stations. Tables 4 and 5 show details of stations that are above sea surface and stations that are on land near the coast, and the data that are available from them to validate input and output accuracy. Observation data were collected every hour; as a result, 744 observations are available for each case and each station. To supplement case 3 – analysis of effects of replacement of topography and land use data on model output of

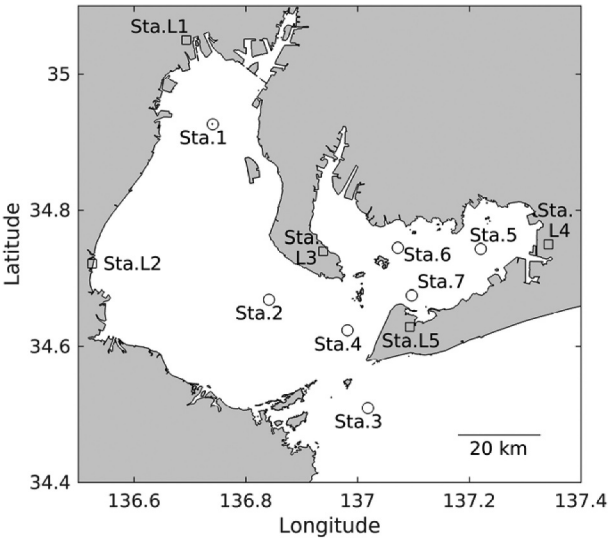

Figure 3. Location of observation stations above sea surface (circles) and on land (squares).

wind speeds and air temperatures – the available observation data over land indicated in Table 5 were used to validate output accuracy.

There is uncertainty in observed wind speeds because of the characteristics of observation equipment when wind speed is low. Thus, in the cases where wind speeds are below 2 m $s^{-1,}$ wind speed data were excluded from the analysis. Observations and model input and output are available at different altitudes; altitude of simulated wind speed was converted to altitude of observed wind speed using Equation (1),

$$W_{zobs} = \begin{cases} W_{10}\left(\frac{z_{obs}}{10}\right)^{\kappa} & z_{obs} \le 10 \\ \frac{W_z\{\log(z_{obs})-\log(10)\}+W_{10}\{\log(z)-\log(z_{obs})\}}{\log(z)-\log(10)} & z_{obs} > 10 \end{cases} \quad (1)$$

where, W_{zobs} (m s^{-1}) is simulated wind speed at the same altitude as the observation, W_{10} (m s^{-1}) is simulated wind speed at 10 m above sea/land surface, W_z (m s^{-1}) is simulated wind speed in the first layer of WRF, z (m) is altitude of the first layer of WRF, z_{obs} (m) is altitude of the observation, κ is a power exponent of the wind profile power law and is set to a value of 0.14. Observations and model input of water temperature, and model input and output of air temperature are also available at different depths, but no conversion was made.

The accuracy of model input data and model output were evaluated using three indices: bias, correlation and root mean square error (RMSE). Improvement Rate (*IR*) of correlation (%), and of RMSE (%) as defined in Equations (2) and (3) were used to evaluate the effects of replacement of input data:

$$IR_{correlation} = \frac{Correlation_{case2to5} - Correlation_{case1}}{Correlation_{case1}} \times 100 \quad (2)$$

Table 4. Details of observation stations above sea surface and the data that are available from them to validate input data and model output accuracy. These observations were conducted by Chubu Regional Bureau, Ministry of Land, Infrastructure, Transport and Tourism and Aichi Fisheries Research Institute (http://www.isewan-db.go.jp/).

Station number	Station name	Latitude (°N)	Longitude (°E)	Altitude of atmospheric observations (m)	Availability of wind speed data		Availability of air temperature data		Depth at which water temperature is measured (m)
					Jan	Jul	Jan	Jul	
1	Back of Ise Bay	34.926	136.741	12.3	N/A	Avail.	Avail.	Avail.	1
2	Center of Ise Bay	34.669	136.841	9.1	Avail.	Avail.	Avail.	N/A	0.5
3	Mouth of Ise Bay	34.509	137.018	13.8	Avail.	Avail.	Avail.	N/A	1
4	Nakayama Channel	34.623	136.982	8.6	Avail.	Avail.	N/A	N/A	1.4
5	No. 1 buoy	34.743	137.220	4.9	Avail.	Avail.	Avail.	Avail.	0.5
6	No. 2 buoy	34.745	137.072	4.9	Avail.	Avail.	Avail.	Avail.	0.5
7	No. 3 buoy	34.675	137.097	4.9	Avail.	Avail.	Avail.	Avail.	0.5

"Avail." indicates that data are available. "N/A" indicates that data are unavailable. Atmospheric observations are obtained from above mean sea level at Stations 1–4, and from above sea surface at Stations 5–7. Water temperatures are obtained from below sea surface at Stations 1, 2, and 5–7, and from below the low water level at Stations 3 and 4.

Table 5. Details of observation stations on land near the coast and the data used to validate input data and model output accuracy. These observations were conducted by Japan Meteorological Agency (https://www.data.jma.go.jp/gmd/risk/obsdl/index.php).

Station number	Station name	Latitude (°N)	Longitude (°E)	Height above sea level (m)	Altitude at which wind speed is measured (m)	Altitude at which air temperature is measured (m)
L1	Kuwana	35.050	136.693	3	10	1.5
L2	Tsu (Wind speed)	34.722	136.525	3	15	-
	Tsu (Temperature)	34.733	136.518	2	-	1.5
L3	Minamichita	34.740	136.938	16	6.5	1.5
L4	Toyohashi	34.750	137.342	3	6.6	1.5
L5	Irago	34.628	137.093	6	10.7	1.5

$$IR_{RMSE} = \frac{RMSE_{case1} - RMSE_{case2to5}}{RMSE_{case1}} \times 100 \quad (3)$$

3. Results

3.1. Validation of input data accuracy

3.1.1. Wind speeds above sea surface

First, input wind speeds above sea surface were validated. Figure 4 shows results of comparisons between observed and input wind speeds averaged over all observation locations above sea surface. Absolute values of the bias of JMA-MA are smaller than those of the NCEP-FNL; correlations of JMA-MA are larger than those of NCEP-FNL; RMSEs of JMA-MA are smaller than those of NCEP-FNL. These results show that, for January and July 2016, wind speeds in JMA-MA are closer than those in NCEP-FNL to measured values.

3.1.2. Temperatures above sea surface

Second, input temperatures above sea surface were validated. Figure 5 is the same as Figure 4, but for temperatures, and shows results averaged over all observation locations. In January, absolute value of the bias of JMA-MA is larger than that of NCEP-FNL; correlation of JMA-MA is larger than that of NCEP-FNL; RMSE of JMA-MA is larger than that of NCEP-FNL. In July, absolute

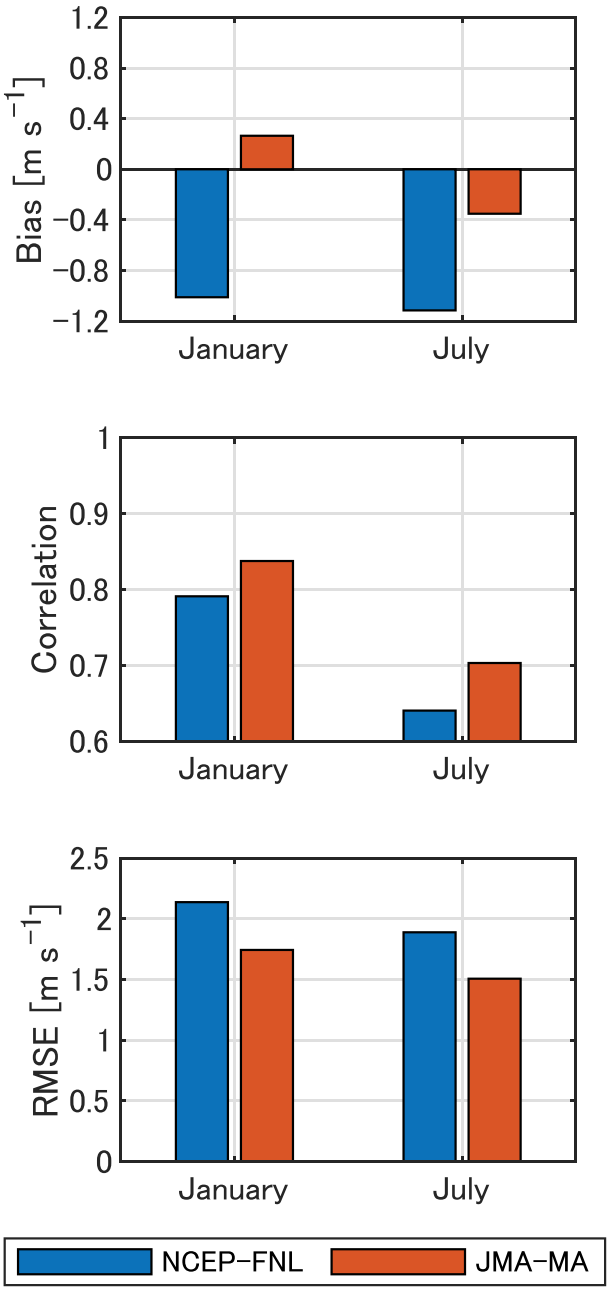

Figure 4. Results of comparisons between observed and input wind speeds. Bar heights indicate mean values of all observation stations above sea surface. Upper: Bias, Center: Correlation, Bottom: RMSE.

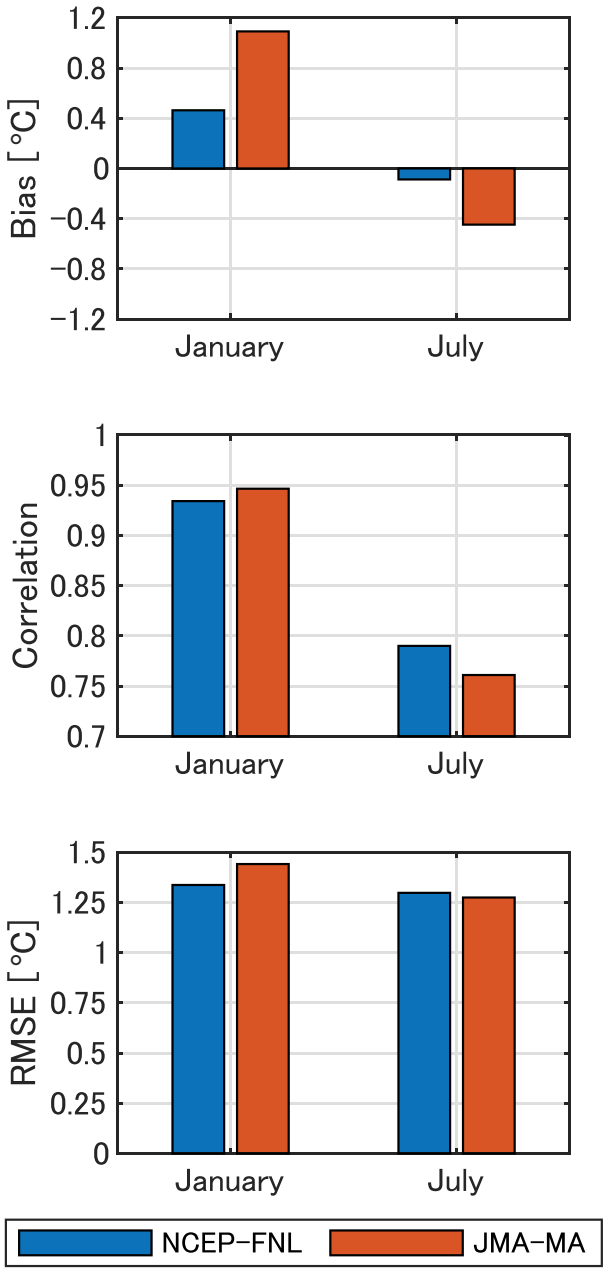

Figure 5. Results of comparisons between observed and input temperatures. Bar heights indicate mean values of all observation stations above sea surface. Upper: Bias, Center: Correlation, Bottom: RMSE.

value of the bias of JMA-MA is larger than that of NCEP-FNL; correlation of JMA-MA is smaller than that of NCEP-FNL; RMSE of JMA-MA is smaller than that of NCEP-FNL. These results show that, for January and July 2016, the accuracy of temperatures in NCEP-FNL was almost the same as that in JMA-MA. However, taking into account all the atmospheric input data variables including the wind field, we judged that JMA-MA reproduces the atmosphere around Ise Bay more accurately than NCEP-FNL because the temperature is affected by advection.

3.1.3. SSTs

Finally, input SSTs were validated. Figure 6 is the same as Figure 4, but for SSTs, and shows results averaged over all observation locations. Absolute values of the bias of JMA-RNWPA are smaller than those of NCEP-FNL; RMSEs of JMA-RNWPA are smaller than those of NCEP-FNL. These results show that, for January and July 2016, JMA-RNWPA has better scores in bias and RMSE of water temperature than NCEP-FNL. This is also the case for correlation in January; correlation of JMA-RNWPA is larger than that of NCEP-FNL. Correlations of both JMA-RNWPA and NCEP-FNL are low in July. Both NCEP-FNL and JMA-RNWPA have large biases in January and small correlations in July. It is difficult to make simple comparisons with observations because of differences between skin and subsurface SST at depth (Donlon et al. 2002). However, overall, we judged that JMA-RNWPA reproduces SST more accurately than NCEP-FNL in January 2016 and that NCEP-FNL and JMA-RNWPA have similar levels of accuracy in July 2016.

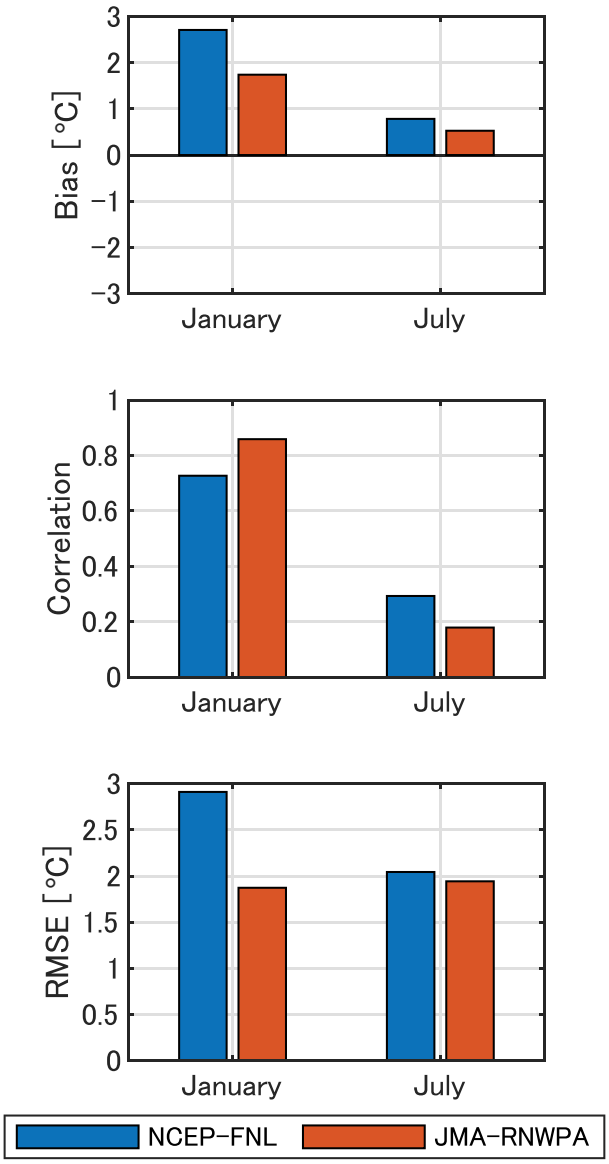

Figure 6. Results of comparisons between observed and input water temperatures. Bar heights indicate mean values of all observation stations. Upper: Bias, Center: Correlation, Bottom: RMSE.

3.2. Validation of simulated wind speed accuracy

Accuracy levels of simulated wind speed were validated. Figure 7 shows results of comparisons between observed and simulated wind speeds averaged over all observation locations above sea surface. Bias, correlation and RMSE in case 5 are similar to those in case 2; among cases 1, 3, and 4, there are no clear differences in bias, correlation or RMSE, indicating that wind speed is mainly affected by atmospheric input data. Difference between bias of case 2 and that of case 1 is positive in both January and July, indicating that replacing NCEP-FNL with JMA-MA results in higher wind speed. This is because bias of JMA-MA is larger than that of NCEP-FNL (Figure 4).

Table 6 shows *IRs* of simulated wind speed. For correlation and RMSE in January and July 2016, *IRs* of case 5 are highest followed by case 2 and those in cases 3 and 4 are much smaller. In summary, replacing default atmospheric input with JMA-MA leads to measurable improvements in simulated wind speed above sea surface. For simulated wind speed, replacing all three default input datasets with region-specific datasets results in an improvement rate of 2.6% in correlation and an improvement rate of 7.1% in RMSE.

Figure 8 shows results of comparisons between observed and simulated wind speeds in cases 1 and 3 averaged over all observation locations on land. In January, absolute value of the bias in case 3 is smaller than that in case 1; in July, absolute value of the bias in case 3 is larger than that in case 1. Correlations of JMA-MA are larger than those of NCEP-FNL; RMSEs of JMA-MA are smaller than those of NCEP-FNL. These results show that, for January and July 2016, simulated wind speeds over land are improved by replacing USGS with GSI.

3.3. Validation of simulated temperature accuracy

Accuracy of simulated temperatures was validated. Figure 9 shows results of comparisons between

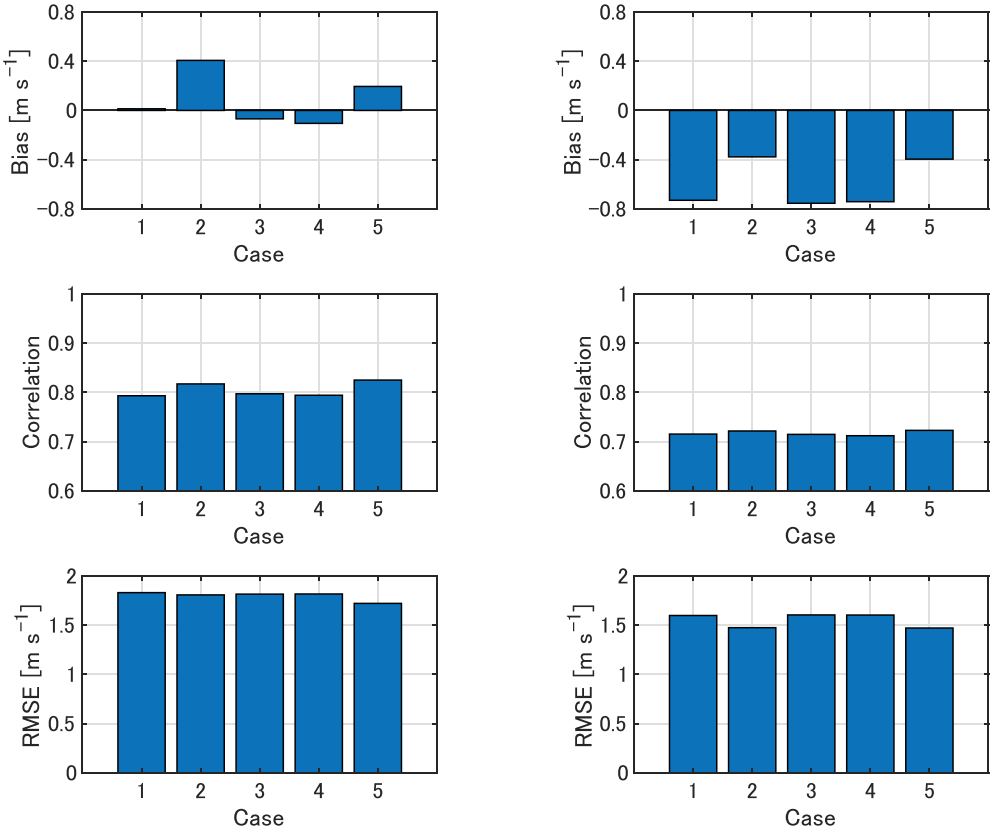

Figure 7. Results of comparisons between observed and simulated wind speeds. Bar heights indicate mean values of all observation stations above sea surface. Upper: Bias, Center: Correlation, Bottom: RMSE. Left: January 2016, Right: July 2016.

Table 6. Improvement rates (*IR*s) of simulated wind speed when default input data are replaced by region-specific input data. Improvement rates were calculated using Equations (2) and (3).

	January		July		Average	
	$IR_{Correlation}$ (%)	IR_{RMSE} (%)	$IR_{Correlation}$ (%)	IR_{RMSE} (%)	$IR_{Correlation}$ (%)	IR_{RMSE} (%)
case 2	3.1	1.5	0.9	7.7	2.0	4.6
case 3	0.6	1.0	0.1	0.4	0.4	0.7
case 4	0.1	0.8	0.5	0.3	0.3	0.5
case 5	4.1	6.2	1.1	8.0	2.6	7.1

observed and simulated temperatures averaged over all observation locations above sea surface. In January, bias, correlation and RMSE in case 5 are similar to those in case 4; bias and RMSE in case 5 are similar to those in case 2; there are no clear differences between cases 1 and 3, indicating that temperature in January is mainly affected by SST and atmospheric input data. On the other hand, in July, bias, correlation and RMSE in case 5 are similar to those in case 2; among cases 1, 3, and 4, there are no clear differences, indicating that temperature in July is mainly affected by atmospheric input data.

Table 7 shows *IR*s of simulated temperature. For RMSE in January, *IR* in case 4 is higher than *IR*s in cases 2 and 3, and for correlation, *IR*s are small in all cases because correlation of case 1 is high (above 0.95). On the other hand, for correlation and RMSE in July, *IR*s in case 2 are higher than those of cases 3 and 4. Therefore, we infer that, out of the three default input datasets, replacing default SST input dataset with JMA-RNWPA is the most effective in improving simulated temperature above sea surface in January, and replacing default atmospheric input dataset with JMA-MA improves simulations for July 2016. For simulated temperature, replacing all three default input datasets with region-specific datasets results in an improvement rate of 3.1% in correlation and an improvement rate of 12.6% in RMSE.

Figure 10 shows results of comparisons over land between observed and simulated temperatures for cases 1 and 3. In January, absolute value of the bias of case 3 is larger than that of case 1; in July, absolute value of the bias of case 3 is smaller than that of case 1. In January, correlation of JMA-MA is the same as that of NCEP-FNL; in July, correlation of JMA-MA is larger than that of NCEP-FNL; RMSEs of JMA-MA are smaller than those of NCEP-FNL. These results show that, for January and July 2016, simulation of temperature over land is improved by replacing USGS with GSI.

4. Discussion

Of all the cases, case 5 has the best scores in correlations and RMSEs for wind speeds and temperatures in January and July (Figures 7 and 9, and Tables 6 and 7). For some input data types, replacement has led to small improvements in model output accuracy. In

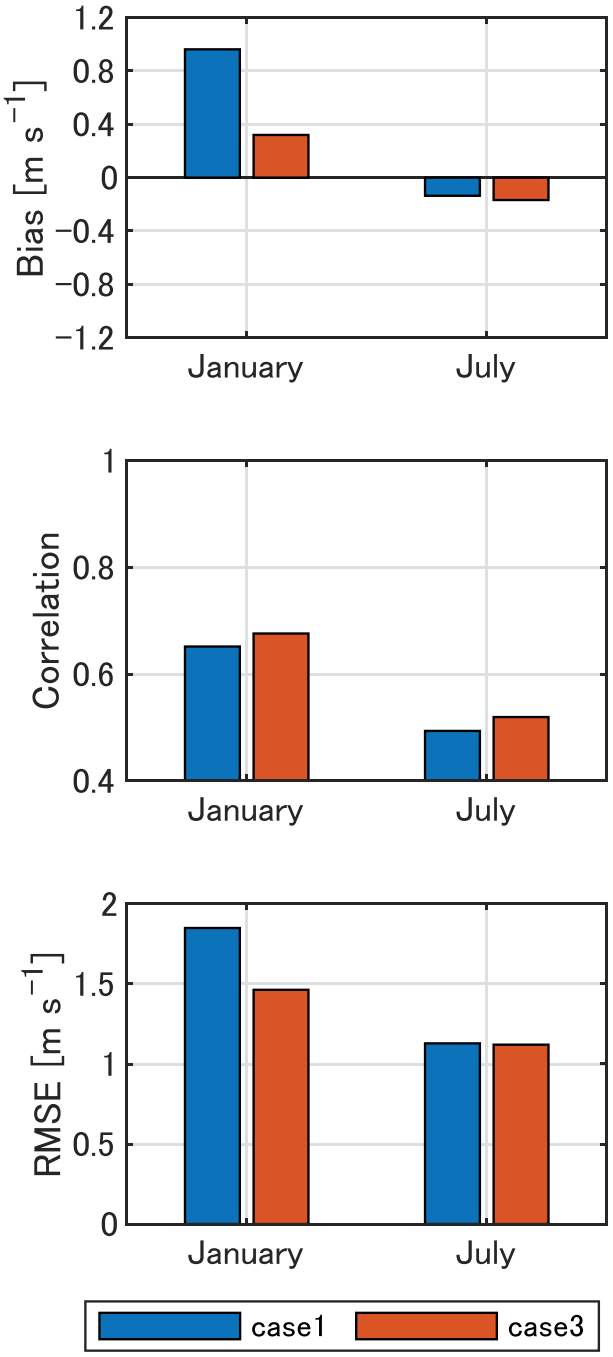

Figure 8. Results of comparisons between observed and simulated wind speeds. Bar heights indicate mean values of all observation stations over land. Upper: Bias, Center: Correlation, Bottom: RMSE.

addition, for WRF simulated temperature, correlation decreases when NCEP-FNL is replaced by JMA-MA, but this could be compensated by replacing other input data. As a result, it is insufficient to consider effects of atmospheric data, topography and land use, and SST separately as in previous studies, and it is important to study combined effects of data replacement as in this study. Improvement of the accuracy of WRF simulations by replacement of input data is discussed in the following sections.

4.1. Sensitivity of simulated wind speed

4.1.1. To atmospheric input data

Wind speeds in JMA-MA are closer than those in NCEP-FNL to measured values (Figure 4). To investigate the process through which replacement of input data improves simulated wind speed, correlations and RMSEs in case 1, case 2, and preliminary simulations were compared. Preliminary simulations were conducted using NCEP-FNL and JMA-MA as atmospheric input data without FDDA following the same procedures as in cases 1 and 2, except without FDDA (referred to as case 1 w/o FDDA and case 2 w/o FDDA). Cases without FDDA highlight the effect of initial and boundary conditions, and comparisons between cases with and without FDDA allow the effect of FDDA to be examined.

In January and July 2016, the accuracy of correlations and RMSEs of case 2 w/o FDDA are higher than those of case 1 w/o FDDA. Thus, correlation and RMSE are improved by the replacement of initial and boundary conditions, with FDDA resulting in greater improvement (Figure 7) (In January 2016, correlation of case 1 w/o FDDA is 0.70, and correlation of case 2 w/o FDDA is 0.72, RMSE of case 1 w/o FDDA is 2.61, and RMSE of case 2 w/o FDDA is 2.59. In July 2016, correlation of case 1 w/o FDDA is 0.53, and correlation of case 2 w/o FDDA is 0.55, RMSE of case 1 w/o FDDA is 2.03, and RMSE of case 2 w/o FDDA is 1.95.).

4.1.2. To topography and land use data

To investigate the process through which replacement of topography and land use data improves model output accuracy, differences between WRF simulated wind speeds for different topography and land use were calculated (case 1 vs case 3). Figure 11 shows root mean square (RMS) differences of simulated wind speeds from cases 1 and 3. The effect of replacing land use data is visible in the grid above land and leeward on the sea surface. Effect of replacing land use data is easily seen in January because seasonal wind blows from land, but is minimal in July because of the land and sea breeze. In areas far from the coast (about 3–8 km from the nearest coastline), RMS differences between wind speeds simulated with different topography and land use input data are small. Closer to the coast (about 2–3 km to the coastline), RMS differences between simulated wind speeds are larger, and are between 0.3 and 0.6 m s^{-1}. It can be inferred from Figures 8 and 11 that accuracy of simulated wind speed at 2–3 km from the coastline is improved by replacing USGS with GSI, although suitable observation data are needed to verify these findings.

Replacement of topography and land use data appears to result in no clear improvement in simulated

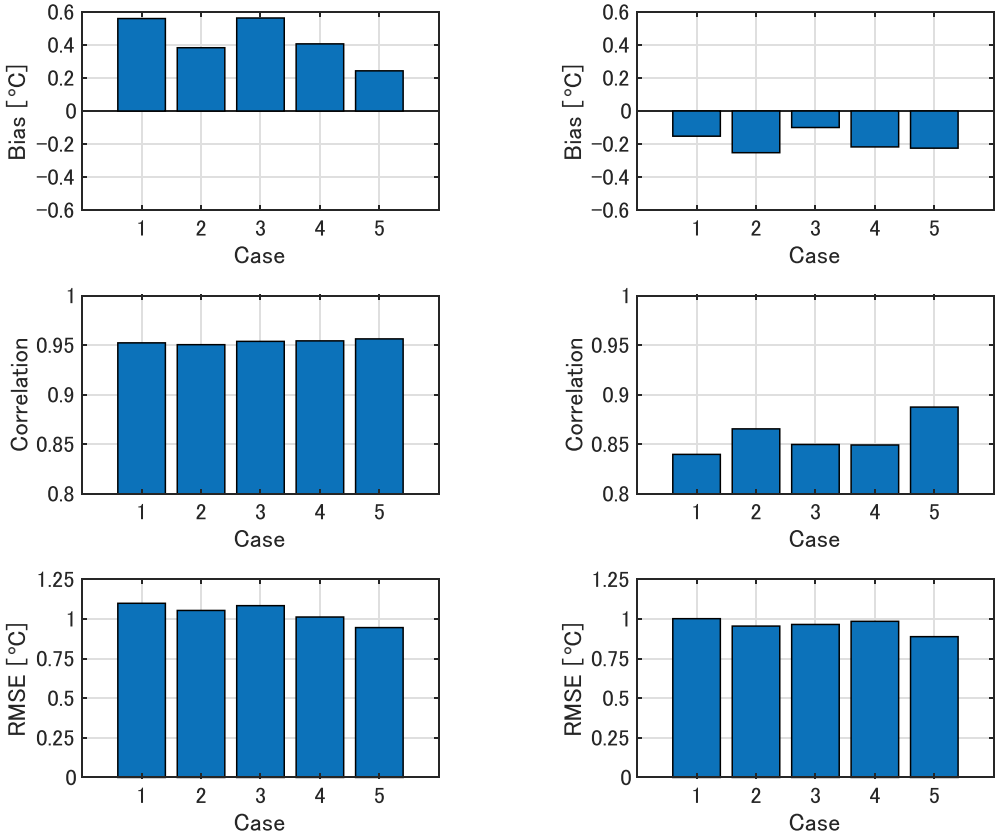

Figure 9. Results of comparisons between observed and simulated temperatures. Bar heights indicate mean values of all observation stations above sea surface. Upper: Bias, Center: Correlation, Bottom: RMSE. Left: January 2016, Right: July 2016.

Table 7. Improvement rates (*IR*s) of simulated air temperature when default input data are replaced by region-specific input data. Improvement rates were calculated using Equations (2) and (3).

	January		July		Average	
	$IR_{Correlation}$ (%)	IR_{RMSE} (%)	$IR_{Correlation}$ (%)	IR_{RMSE} (%)	$IR_{Correlation}$ (%)	IR_{RMSE} (%)
case 2	−0.2	4.1	3.1	4.7	1.4	4.4
case 3	0.2	1.4	1.2	3.6	0.7	2.5
case 4	0.2	7.9	1.1	1.7	0.7	4.8
case 5	0.4	14.0	5.7	11.3	3.1	12.6

wind speed accuracy, which differs from the findings of Kikuchi, Fukushima, and Ishihara (2020) that indicate that replacement of land use data reduced overestimation of speed of the wind from the north (blowing from land to sea) at an observation station (meteorological mast) 3.1 km from the coastline. Discrepancy between these findings appears to be related to the positions of the observation stations in the two studies. While the two studies focused on different land use data and study areas, the offshore observation station in Kikuchi, Fukushima, and Ishihara (2020) is near to land and its distance from the coast (3.1 km) is almost within the range (2–3 km) in which simulated wind speed accuracy is improved by replacing USGS with GSI in this study.

Next, we focused on a strong wind event to examine the effects of different topography and land use data on the wind field. There was a strong northwesterly wind in January 2016 with wind speeds of over 15 m s^{-1} above the sea surface averaged over 24 hours (Figure 12). For case 1, the coastal areas, small islands, and offshore airport in case 3 were set to sea. Difference between averaged wind speed in case 3 and that in case 1 shows the effect of different topography and land use, and wind speed in case 3 is lower than that in case 1 in these areas (Figure 13). Therefore, changes in topography and land use data will have impacts at locations where sea and land settings are misconfigured.

4.1.3. To SST

Replacement of NCEP-FNL by JMA-RNWPA as the source of SST input data appears to result in no clear improvement, which differs from the findings of Shimada et al. (2015). In their study of sensitivity of WRF simulated offshore wind speed to SST input, Shimada et al. (2015) concluded that the use of SST input that is close to measured values is key for achieving realistic simulations of offshore wind above sea surface. They conducted simulations over the whole year of 2011, and used SST values from NCEP-FNL and MOSST, which is the MODIS SST product of JAXA (Hosoda et al. 2007; Shimada et al. 2015). In MOSST, the bias of water temperature had been corrected with in-situ seawater temperature at a depth of 0.3 m. The WRF model domain was over western Japan, including Osaka Bay, which is 150 km to the west of Ise Bay, and has almost the same size as Ise Bay.

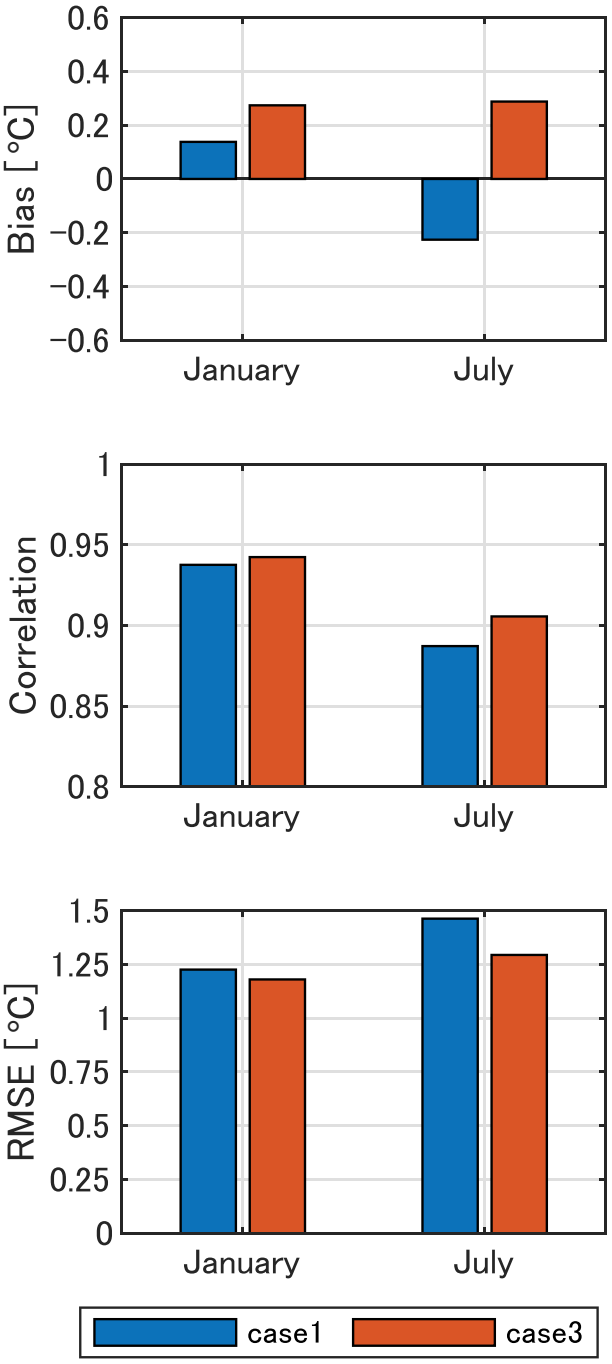

Figure 10. Results of comparisons between observed and simulated temperatures. Bar heights indicate mean values of all observation stations over land. Upper: Bias, Center: Correlation, Bottom: RMSE.

We calculated the improvement ratio – the ratio of difference in simulated wind speed RMSE to difference in SST RMSE as a result of replacement of SST input – from the results of Shimada et al. (2015) and those of this study. We calculated average RMSEs of SST and simulated wind speed in Osaka Bay using data from the bar graphs in Figures 6 and 10 of Shimada et al. (2015); RMSEs of SST are 4.7°C (NCEP-FNL) and 1.1°C (MOSST), and RMSEs of simulated wind speed are 2.5 m s^{-1} (NCEP-FNL) and 2.1 m s^{-1} (MOSST). Thus, improvement ratio of simulated wind speed when NCEP-FNL is replaced by MOSST as the source of SST input data is calculated as: (2.5 – 2.1)/(4.7 – 1.1) = 0.11. From our simulations, average RMSEs of SST are 2.5°C (NCEP-FNL) and 1.9°C (JMA-RNWPA), and average RMSEs of simulated wind speeds are 1.76 m s^{-1} (NCEP-FNL) and 1.68 m s^{-1} (JMA-RNWPA). Thus, improvement ratio of simulated wind speed when NCEP-FNL is replaced by JMA-RNWPA as the source of SST input data is calculated as: (1.76 – 1.68)/(2.5 – 1.9) = 0.13. The improvement ratio calculated from the data in Shimada et al. (2015) has almost the same value as the improvement ratio from our simulations, indicating that replacing default SST with region-specific dataset improves simulation of wind speed.

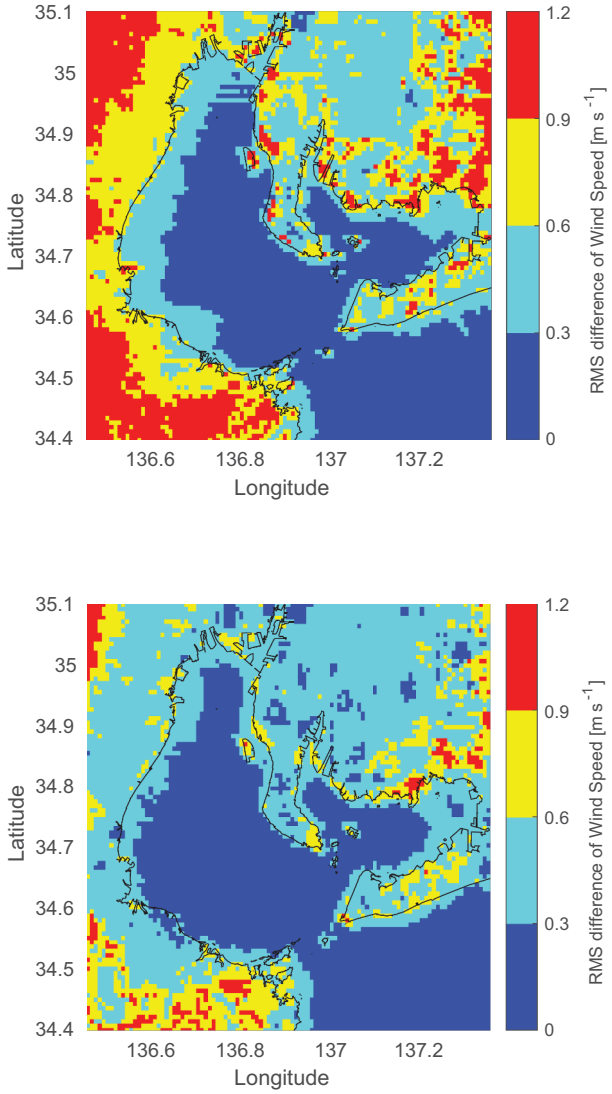

Figure 11. Root mean square differences between simulated wind speed from case 1 and simulated wind speed from case 3. Upper: January 2016, Lower: July 2016. Black line indicates coastline.

4.2. Sensitivity of simulated temperature

4.2.1. To atmospheric input data

Replacement of NCEP-FNL with JMA-MA atmospheric input data improves correlation of simulated temperatures in July and RMSEs of simulated temperatures in

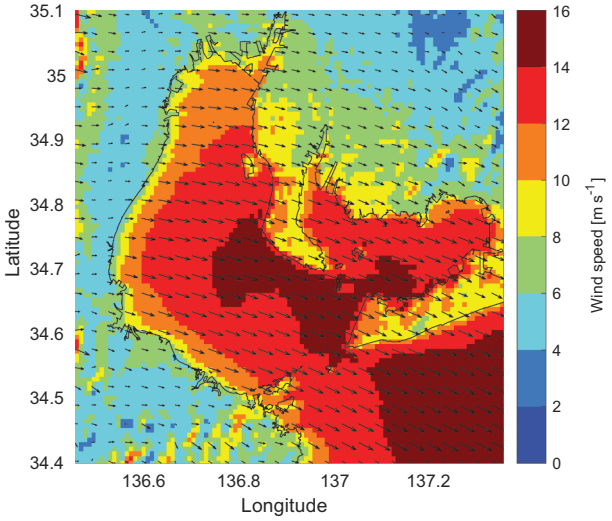

Figure 12. Plane view of wind speed and direction in case 3 averaged between 15:00 UTC January 18 and 14:00 UTC January 19 2016. Vectors indicate wind directions. Black line indicates coastline.

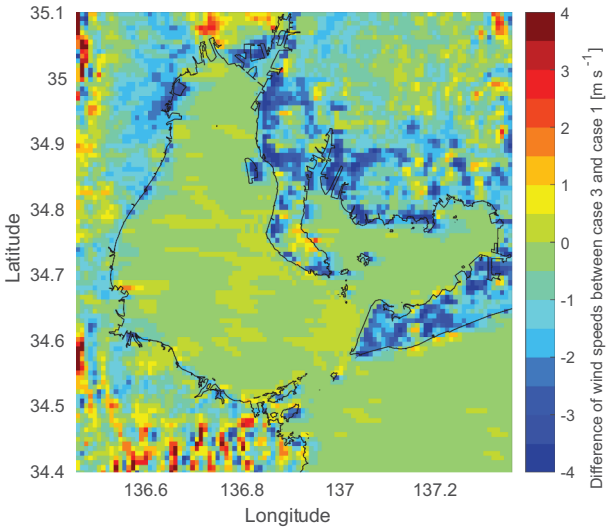

Figure 13. Plane view of difference between wind speed in case 3 and wind speed in case 1 averaged between 15:00 UTC January 18 and 14:00 UTC January 19 2016. Black line indicates coastline.

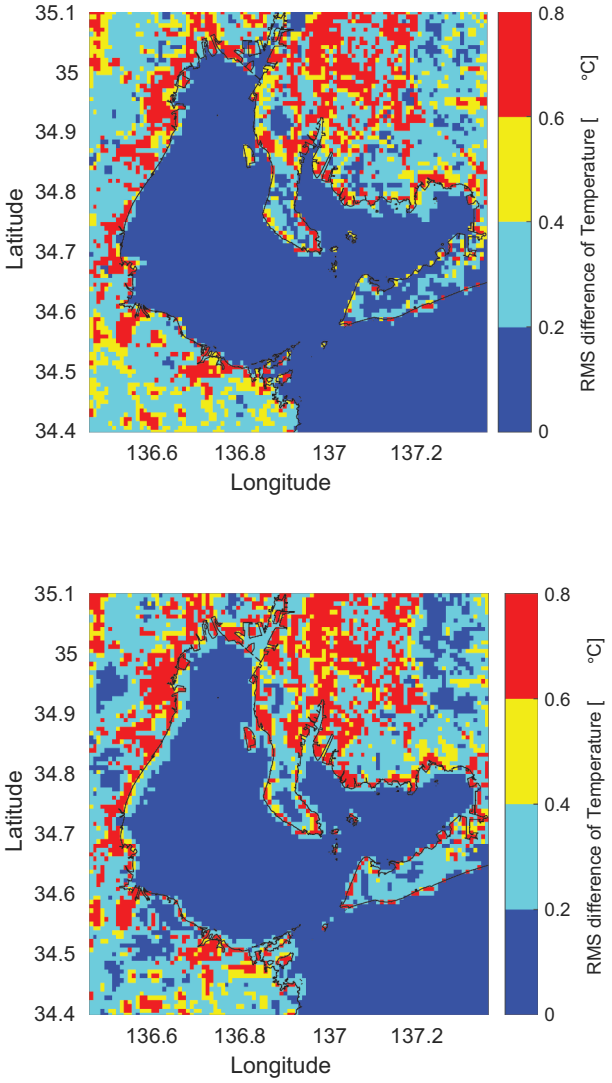

Figure 14. Root mean square differences between simulated temperature from case 1 and simulated temperature from case 3. Upper: January 2016, Lower: July 2016. Black line indicates coastline.

January and July (Figure 9), possibly because of the high accuracy of the input data. To investigate the process through which replacement of the input data improves simulations of temperature, we compared correlations and RMSEs of the preliminary simulations from Section 4.1.1.

In January 2016, the accuracy of RMSE of case 2 w/o FDDA are lower than those of case 1 w/o FDDA. Thus, for January 2016, RMSE is improved by FDDA (Figure 9) but not by replacement of initial and boundary conditions. In July 2016, the accuracy of correlation and RMSE of case 2 w/o FDDA are higher than those of case 1 w/o FDDA. Thus, for July 2016, correlation and RMSE are improved by replacement of initial and boundary conditions, with FDDA resulting in greater improvement (Figure 9) (In January 2016, correlation of case 1 w/o FDDA is 0.92, and correlation of case 2 w/o FDDA is 0.92, RMSE of case 1 w/o FDDA is 1.26, and RMSE of case 2 w/o FDDA is 1.36. In July 2016, correlation of case 1 w/o FDDA is 0.74, and correlation of case 2 w/o FDDA is 0.76, RMSE of case 1 w/o FDDA is 1.23, and RMSE of case 2 w/o FDDA is 1.19.).

4.2.2. To topography and land use data

Differences between WRF simulated temperatures for different topography and land use were calculated (case 1 vs case 3) using the same method as that described in Section 4.1.2. Figure 14 shows RMS differences of simulated temperatures from cases 1 and 3. Above sea surface near the coast (within about 2 km of the coastline), RMS differences between simulated temperatures are between 0.2 and 0.4°C, which are larger than those further from the coast.

It can be inferred from Figures 10 and 14 that accuracy of simulated temperature within 2 km from

the coastline is improved by replacing USGS with GSI, although suitable observation data are needed to verify these findings. Therefore, replacement of topography and land use data improves simulated temperature accuracy over land and above sea surface near the coastline; however, improvements are restricted to locations near the coast.

4.2.3. To SST

Differences in simulated temperature improvement between January and July are caused by accuracy of SST input data (Figure 6). In January, temperature simulated with JMA-RNWPA has better scores than that simulated with NCEP-FNL; in July, there is no clear difference between the accuracies of temperatures simulated using different input data.

4.3. Limits of applicability

Limits of applicability of our study results are described below.

4.3.1. Robustness and generalizability of results

The WRF simulations were conducted for January and July 2016. However, error in WRF simulated wind speed and temperature may have different magnitudes in different years and seasons. There were no extreme phenomena (e.g. typhoons) in January and July 2016; therefore, extreme phenomena are also absent from our analyses. More simulations are needed to enhance robustness and generalizability of WRF simulation results and to understand the factors underlying differences in magnitudes of errors.

4.3.2. Relationship between simulation setup and study results

Results from WRF simulations vary according to simulation setup. For example, simulations with and without FDDA produce completely different results (Sections 4.1.1 and 4.2.1). However, this was not the focus of this study, and variation of scores and the improvement rate with simulation setup need to be considered in future studies.

5. Conclusions

Sensitivity of model output above sea surface to the replacement of default input dataset with region-specific dataset is unknown; in particular, it is unclear which input data type, when replaced, results in large improvements in WRF simulation results around Japan. In this study, WRF simulations were conducted for Ise Bay, Japan for the entire months of January and July 2016. Three region-specific input datasets were used to evaluate sensitivity of model output above sea surface to the replacement of default input datasets. Accuracies of simulated wind speeds and temperatures were evaluated by comparing simulation output with observation data collected above the sea surface in Ise Bay.

Replacement of atmospheric input data from NCEP-FNL with JMA-MA results in improvement of accuracies in simulated wind speed and temperature because JMA-MA values are closer than those in NCEP-FNL to measured values. Of the three region-specific datasets, replacement of atmospheric input data from NCEP-FNL with those in JMA-MA results in the largest improvements in simulated wind speeds in January and July, and in simulated temperature in July 2016.

For areas far from the coast, simulated wind speed and temperature accuracies show no clear improvement when USGS is replaced with GSI as the source of topography and land use data; near the coast, replacement of input data results in improvements in simulated wind speed and temperature.

Simulated wind speed accuracy shows no clear improvement when NCEP-FNL is replaced with JMA-RNWPA as the source of SST input data in July because NCEP-FNL and JMA-RNWPA have similar levels of accuracy. However, accuracy of simulated temperature in January is improved when NCEP-FNL is replaced with JMA-RNWPA; therefore, SST input data that are representative of local conditions improve the accuracy of simulated temperature. Of the three region-specific datasets, replacement of NCEP-FNL with JMA-RNWPA as the source of SST input data results in the largest improvements in simulated temperatures in January 2016.

Replacing all three default input datasets with region-specific datasets results in *IR*s (improvement rates) in wind speed of 2.6% in correlation and 7.1% in RMSE; *IR*s in temperature are 3.1% in correlation and 12.6% in RMSE. Replacing all three default input datasets results in the highest improvement rates. Our study shows that replacement of all default input datasets with region-specific datasets is important for accurate simulations using WRF. It expands on previous studies that focused on the effects of replacing only one input data type at a time.

Acknowledgments

This study was funded by the Port and Airport Research Institute. Observed wind, air temperature above sea surface, and water temperature data were obtained from Chubu Regional Bureau, Ministry of Land, Infrastructure, Transport and Tourism, and Aichi Fisheries Research Institute. Observed wind and air temperature on land were obtained from Japan Meteorological Agency. We extend thanks to Dr. T. Kobayashi of Gifu University, Dr. T. Ohsawa of Kobe University, Dr. S. Shimada of National Institute of Advanced Industrial Science and Technology, Dr. Y. Takeyama of Tokyo University of Marine Science and Technology, Dr. K. Suzuyama of Ecoh Corporation, Mr. K. Koike of Idea Consultants, Inc., Dr. K. Matsuura of Japan Weather Association, and Dr. T. Takagawa of the Port and Airport

Research Institute for their advice on our study. We thank Tina Tin, Ph.D., from Edanz Group (https://en-author-services.edanzgroup.com/ac), for editing a draft of this manuscript.

Disclosure statement

No potential conflict of interest was reported by the authors.

ORCID

Yoshitaka Matsuzaki http://orcid.org/0000-0003-1040-0916
Takashi Fujiki http://orcid.org/0000-0001-8415-3087
Tetsunori Inoue http://orcid.org/0000-0002-1308-5344

References

Akimoto, Y., and H. Kusaka. 2010. "Sensitivity of the WRF Regional Meteorological Model to Input Datasets and Surface Parameters for the Kanto Plain on Fine Summer Days." *Geographical Review of Japan Series A* 83 (3): 324–340. doi:10.4157/grj.83.324.

Carvalho, D., A. Rocha, and M. Gómez-Gesteira. 2012. "Ocean Surface Wind Simulation Forced by Different Reanalyses: Comparison with Observed Data along the Iberian Peninsula Coast." *Ocean Modelling* 56: 31–42. doi:10.1016/j.ocemod.2012.08.002.

Cheng, F.-Y., Y.-C. Hsu, P.-L. Lin, and T.-H. Lin. 2013. "Investigation of the Effects of Different Land Use and Land Cover Patterns on Mesoscale Meteorological Simulations in the Taiwan Area." *Journal of Applied Meteorology and Climatology* 52: 570–587. doi:10.1175/JAMC-D-12-0109.1.

Donlon, C. J., P. J. Minnett, C. Gentemann, T. J. Nightingale, I. J. Barton, B. Ward, and M. J. Murray. 2002. "Toward Improved Validation of Satellite Sea Surface Skin Temperature Measurements for Climate Research." *Journal of Climate* 15 (4): 353–369. doi:10.1175/1520-0442-(2002)015<0353:TIVOSS>2.0.CO;2.

Gemmill, W., B. Katz, and X. Li. 2007. "*Daily Real-time, Global Sea Surface temperature—High-resolution Analysis: RTG_SST_HR*." NOAA/NWS/NCEP/EMC/MMAB, Science Application International Corporation, and Joint Center for Satellite Data Assimilation Technical Note No. 260. https://polar.ncep.noaa.gov/mmab/papers/tn260/MMAB260.pdf

Higa, H., Y. Koibuchi, H. Kobayashi, M. Toratani, and Y. Sakuno. 2015. "Numerical Simulation and Remote Sensing for the Analysis of Blue Tide Distribution in Tokyo Bay in September 2012." *Journal of Advanced Simulation in Science and Engineering* 2: 1–15. doi:10.15748/jasse.2.1.

Hosoda, K., H. Murakami, F. Sakaida, and H. Kawamura. 2007. "Algorithm and Validation of Sea Surface Temperature Observation Using MODIS Sensors aboard Terra and Aqua in the Western North Pacific." *Journal of Oceanography* 63: 267–280. doi:10.1007/s10872-007-0027-4.

Japan Meteorological Agency. 2016. "*Training Text of Numerical Simulation on 2016*." Report No. 49. https://www.jma.go.jp/jma/kishou/books/nwptext/49/No49_all.pdf

Jee, J.-B., and S. Kim. 2016. "Sensitivity Study on High-resolution Numerical Modeling of Static Topographic Data." *Atmosphere* 7 (7): 86. doi:10.3390/atmos7070086.

Jiménez-Esteve, B., M. Udina, M. R. Soler, N. Pepin, and J. R. Miró. 2018. "Land Use and Topography Influence in A Complex Terrain Area: A High Resolution Mesoscale Modelling Study over the Eastern Pyrenees Using the WRF Model." *Atmospheric Research* 202: 49–62. doi:10.1016/j.atmosres.2017.11.012.

Kikuchi, Y., M. Fukushima, and T. Ishihara. 2020. "Assessment of a Coastal Offshore Wind Climate by Means of Mesoscale Model Simulations considering High-resolution Land Use and Sea Surface Temperature Data Sets." *Atmosphere* 11: 4. doi:10.3390/atmos11040379.

LaCasse, K. M., M. E. Splitt, S. M. Lazarus, and W. M. Lapenta. 2008. "The Impact of High-resolution Sea Surface Temperatures on the Simulated Nocturnal Florida Marine Boundary Layer." *Monthly Weather Review* 136: 1349–1372. doi:10.1175/2007MWR2167.1.

Lai, Z., R. Ma, M. Huang, C. Chen, Y. Chen, C. Xie, and R. C. Beardsley. 2016. "Downwelling Wind, Tides, and Estuarine Plume Dynamics." *Journal of Geophysical Research: Oceans* 121: 4245–4263. doi:10.1002/2015JC011475.

Loveland, T. R., B. C. Reed, J. F. Brown, D. O. Ohlen, Z. Zhu, L. Yang, and J. W. Merchant. 2000. "Development of a Global Land Cover Characteristics Database and IGBP DISCover from 1 Km AVHRR Data." *International Journal of Remote Sensing* 21: 1303–1330. doi:10.1080/014311600210191.

Mallard, M. S., T. L. Spero, and S. M. Taylor. 2018. "Examining WRF's Sensitivity to Contemporary Land-use Datasets across the Contiguous United States Using Dynamical Downscaling." *Journal of Applied Meteorology and Climatology* 57: 2561–2583. doi:10.1175/JAMC-D-17-0328.1.

Maturi, E., A. Harris, J. Mittaz, J. Sapper, G. Wick, X. Zhu, P. Dash, and P. Koner. 2017. "A New High-resolution Sea Surface Temperature Blended Analysis." *Bulletin of the American Meteorological Society* 98: 1015–1026. doi:10.1175/BAMS-D-15-00002.1.

Misaki, T. T., M. Ohsawa, S. Konagaya, Y. Shimada, Y. Takeyama, and S. Nakamura. 2019. "Accuracy Comparison of Coastal Wind Speeds between WRF Simulations Using Different Input Datasets in Japan." *Energies* 12 (14): 2754. doi:10.3390/en12142754.

National Centers for Environmental Prediction/National Weather Service/NOAA/U.S. Department of Commerce. 2015. "NCEP GDAS/FNL 0.25 Degree Global Tropospheric Analyses and Forecast Grids." Accessed 18 September 2019. doi:10.5065/D65Q4T4Z.

Sashiyama, S., and K. Yamamoto. 2014. "Method for Evaluating the Influence of Obstruction of Sea Breeze by Clusters of High-rise Buildings on the Urban Heat Island Effect." *Journal of Environmental Protection* 5: 983–996. doi:10.4236/jep.2014.511099.

Sekine, Y., S. Nakamura, and Y. W. Wang. 2002. "Variation in Wind in the Region around Ise Bay." *The Bulletin of the Faculty of Bioresources, Mie University* 28: 1–9.

Sertel, E., A. Robock, and C. Ormeci. 2010. "Impacts of Land Cover Data Quality on Regional Climate Simulations." *International Journal of Climatology* 30: 1942–1953. doi:10.1002/joc.2036.

Shimada, S., T. Ohsawa, T. Kogaki, G. Steinfeld, and D. Heinemann. 2015. "Effects of Sea Surface Temperature Accuracy on Offshore Wind Resource Assessment Using a Mesoscale Model: Effects of SST Accuracy on Offshore Wind Simulations." *Wind Energy* 18: 1839–1854. doi:10.1002/we.1796.

Skamarock, W., J. Klemp, J. Dudhia, D. Gill, D. Barker, W. Wang, X.-Y. Huang, and M. Duda. 2008. "*A Description of the Advanced Research WRF Version 3*." NCAR Technical Note NCAR/TN-475+STR. doi:10.5065/D68S4MVH.

Song, Q., D. B. Chelton, S. K. Esbensen, N. Thum, and L. O'Neill. 2009. "Coupling between Sea Surface Temperature and Low-level Winds in Mesoscale Numerical Models." *Journal of Climate* 22 (1): 146–164. doi:10.1175/2008JCLI2488.1.

Thiébaux, J., E. Rogers, W. Wang, and B. Katz. 2003. "A New High-resolution Blended Real-time Global Sea Surface Temperature Analysis." *Bulletin of the American Meteorological Society* 84: 645–656. doi:10.1175/BAMS-84-5-645.

Usui, N., S. Ishizaki, Y. Fujii, H. Tsujino, T. Yasuda, and M. Kamachi. 2006. "Meteorological Research Institute Multivariate Ocean Variational Estimation (MOVE) System: Some Early Results." *Advances in Space Research* 37: 806–822. doi:10.1016/j.asr.2005.09.022.